Topic 11. Computer tools and experimental techniques for assessment of building energy and built environment

# Validation of Three Dimensional Fast Fluid Dynamics for Indoor Airflow Simulations

Mingang Jin [1], Wangda Zuo [2], and Qingyan Chen[1*]

[1]School of Mechanical Engineering, Purdue University, West Lafayette, IN 47907, USA
[2]Environmental Energy Technologies Division, Lawrence Berkeley National Laboratory, Berkeley, CA 94720, USA

[*]*Corresponding email: yanchen@purdue.edu*

*Keywords: Fast fluid dynamics; Building airflow simulations; Boundary condition*

## SUMMARY

Real time simulations of airflow in buildings could provide better opportunities for designing and controlling indoor environment. Fast Fluid Dynamics (FFD) could be potentially used for real-time indoor airflow simulations. This study developed two-dimensional Fast Fluid Dynamics (2D FFD) into three-dimensional Fast Fluid Dynamics (3D FFD). The implementation of boundary condition at outlet was improved with local mass conservation method, and a near-wall treatment for Semi-Lagrangian scheme was applied to avoid having departure points located outside the boundary. This study tested 3D FFD with three cases of indoor airflows with increasing complexity. Compared with the high quality experimental data, the numerical results showed that 3D FFD could capture general airflow features and provide reliable and accurate simulations for airflows in buildings. The computing speed was about 15 times faster than CFD.

## INTRODUCTION

Real time simulations of airflow in buildings could provide better opportunities in designing and controlling indoor environment. Although Computational Fluid Dynamics (CFD) has the potential to be used for the airflow simulations, CFD is too slow with the present computing power in most of the design firms (Zhai and Chen 2006; Chen 2009). On the other hand, multi-zone network models could significantly decrease the computing time so that real time or faster-than-real-time simulations are possible. But it might not be valid for large indoor spaces with stratified ventilation systems (Wang and Chen 2008), and it also uses only one node for a room that provides insufficient information of the micro environment. As an intermediate approach between computational fluid dynamics (CFD) and multi-zone model, fast fluid dynamics (FFD) can achieve informative airflow simulations with fast speed so that it has the potential to perform real-time indoor airflow simulations. Zuo and Chen (2009) developed a two-dimensional Fast Fluid Dynamics (2D FFD) for airflow simulations in buildings. Their results show that the computing speed was 50 times faster than CFD and real-time simulation of indoor airflow seems possible. Although the results were not as accurate as those of CFD, they were much better than those produced by the multi-zone model.

However, flows in buildings are complex and always three dimensional (Zhai et al. 2007). In order to capture the characteristics of the three-dimensional airflows, it is necessary to extend

the 2D FFD code into a three dimensional one. To demonstrate the capabilities and accuracy of the 3D FFD code, it is essential to validate it with a few cases of indoor airflows.

## METHODS

### Governing equations for fast fluid dynamics

Fast Fluid Dynamics is a technique introduced by Stam (1999) for computer games, aimed to simulate incompressible fluid flows by solving the incompressible Navier-Stokes (NS) equations (1) and continuity equation (2) with a simple and stable approach.

$$\frac{\partial U_i}{\partial t}+U_j\frac{\partial U_i}{\partial x_j}=-\frac{1}{\rho}\frac{\partial p}{\partial x_i}+\upsilon\frac{\partial^2 U_i}{\partial x_j\partial x_j}+\frac{1}{\rho}F_i \quad (1)$$

$$\frac{\partial U_i}{\partial x_i}=0 \quad (2)$$

where $U_i$ and $U_j$ are velocity, p pressure, ρ density, $F_i$ body forces, and $x_i$ and $x_j$ spacial coordinates, respectively. In FFD, instead of solving a coupled system of Navier-Stokes equations for velocity and pressure, the time-splitting method is applied to sequentially solve the advection equations and diffusions equations. The obtained intermediate velocity field is then projected into a space of divergence free vector field through pressure projection. After obtaining the velocity field, transport equations for other scalars can be further solved similarly.

### Boundary conditions

In FFD, paired boundary conditions for both velocity and pressure are required to solve implicit diffusion equations and pressure projection equation (Temam 1991; Kim and Lee 2002). For airflow simulations in buildings, the computation domains are typically bounded by solid walls and openings, such as inlets and outlets. For the solid walls, non-slip boundary is usually applied. For inlets, constant velocity is enforced. Both of these two boundary conditions can be categorized as Dirichlet boundary. As equation (3) shows, the 3D FFD used the physical velocity boundary condition as boundary condition for intermediate velocity. The Neumann boundary condition for pressure was applied as shown by equation (4).

$$U_i^{**}|_b=U_i^{n+1}|_b=U_{bi} \quad (3)$$

$$\frac{\partial p}{\partial n}|_b=0 \quad (4)$$

At outlets, usually outflow boundary condition is applied. This investigation applied the local mass conservation for the outflow boundary conditions for velocity as suggested by Li and Tao (1994). Figure 1 illustrated the implementation of local mass conservation method. The normal derivative of tangential velocity at the outlet was set to zero. The velocity component normal to the outlet was firstly derived by applying mass conservation at the cells adjacent to the outlet, as shown in equation (5).

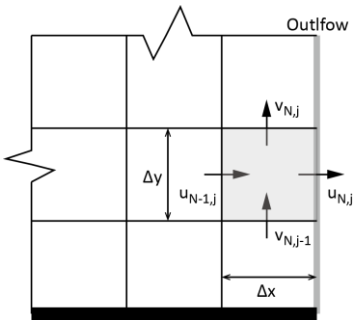


*Figure 1 Boundary control volume for local mass conservation method*

$$u_{N,j} = u_{N-1,j} + \frac{\Delta x}{\Delta y}(v_{N,j-1} - v_{N,j}) \tag{5}$$

However the boundary velocity derived from equation (10) would not ensure overall mass conservation. This study further corrected the boundary normal velocity through mass correction equation (6).

$$u_{N,j} = u_{N,j} \times \frac{Mass_{in}}{Mass_{out}} \tag{6}$$

where, $Mass_{in}$ is the total mass-flow rate at all the inlets and $Mass_{out}$ the total mass-flow rate at all the outlets, respectively. Since the mass conservation constraint had already been applied at the outlet boundary cells, it was not necessary to update the normal velocity at the outlet boundary through pressure projection. Similarly, Neumann boundary conditions could be derived for pressure at outflow boundaries as shown by equation (4).

**Treatment of Semi-Lagrangian scheme at near-wall regions**

The truncation error of Semi-Lagrangian scheme might lead to unrealistic results that the flow near a solid wall could be traced back outside the flow field (Wood et al. 2009). In order to avoid this, the 3D FFD employed a special treatment for the Semi-Lagrangian scheme at the near wall region. The treatment assumed that the velocity component normal to the wall varied linearly between the wall boundary and the first grid adjacent to the wall, as shown in Figure 2(a). If the backward trajectory crossed the first grid close to the wall boundary, the tracing back velocity in the normal wall direction would linearly decrease to zero at wall surface. Thus the departure point would not locate outside the domain.

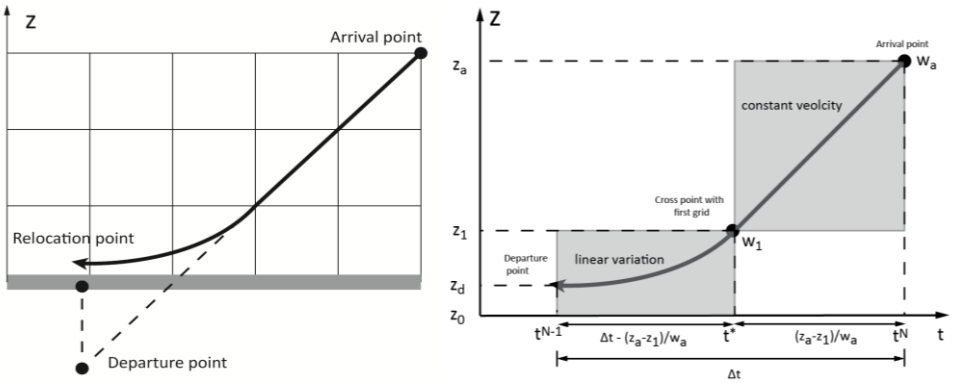


(a) (b)

*Figure 2 Schematic of near wall treatment for the Semi-Lagrangian scheme*

As illustrated in Figure 2(b), the trace back in the normal wall direction (z direction) was first performed with velocity at arrival point, which was $w_a$. Once the trace back trajectory crossed the first grid adjacent to the wall, the equation (7) was used for trace back velocity, w.

$$w=\frac{z-z_0}{z_1-z_0}w_1 \tag{7}$$

where, z is coordinate in normal wall direction, $z_0$ the coordinate of wall boundary in normal wall direction, $z_1$ the coordinate of first grid adjacent to wall in normal wall direction and w1 the velocity at the point where the trajectory crossed the first grid adjacent to the wall, respectively. The equation (7) was then integrated over the remained trace-back time to derive the coordinate of departure point, as shown by equation (8).

$$z_d=z_0+(z_1-z_0)\exp\left[-\frac{v_1}{z_1-z_0}(\Delta t-\frac{z_a-z_1}{w_a})\right] \tag{8}$$

where z is the coordinate of departure point in normal wall direction, $z_a$ the coordinate of arrival point in normal wall direction and $\Delta t$ the time step size, respectively.

## RESULTS

This investigation evaluated the performance of the 3D FFD with three cases of indoor airflows having increasing complexity: (1) a forced convection flow in empty room, (2) a forced convection flow in a room with a box that represents a piece of furniture, and (3) a mixed convection flow in a room with a heated box that represents occupant or heated equipment. The experimental data were from Wang and Chen (2009).

### Forced convection in the empty room

As shown in Figure 3, an isothermal jet was generated at the inlet at upper left corner and developed along the ceiling, reaching far right. The air then turned downwards because of the existence of right wall and further formed a circulation in the room. This was a basic airflow pattern in a mechanically ventilated room. The room size was 2.44 m × 2.44 m × 2.44 m and the inlet and outlet height was 0.03 m and 0.08 m, respectively. The inlet air velocity was 0.455 m/s in studies by Wang and Chen (2009). The corresponding Reynolds number is 2600, which indicates that the flow was transitional. In order to compare the performance of 3D FFD with CFD tools, the laminar CFD simulation using ANSYS Fluent 12.1 was also performed for this test case. The grid size of 20×20×20 was used for both 3D FFD and laminar CFD calculations.

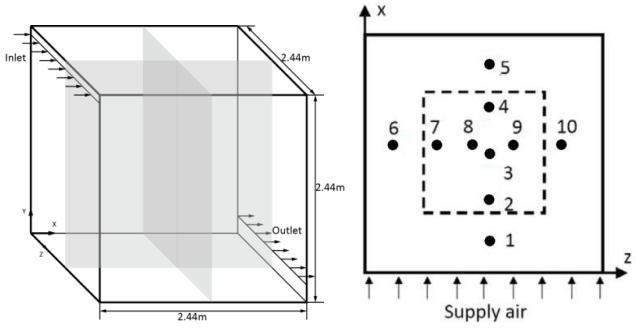


(a) (b)

*Figure 3 Schematic of the test chamber for the forced convection and measurement positions*

Figure 4 showed the velocity profiles at four measurement positions predicted by 3D FFD and laminar CFD. As depicted in Figure 3, the four positions were 1, 3, 5 and 6 located at the jet upstream, jet downstream, room center and a position close to the side wall, respectively. Figure 4 showed that 3D FFD predicted similar airflow as the laminar CFD in this case. Both of them could predict general velocity variation in the vertical direction and capture the high speed of the jet from inlet. Their results matched with experimental data quite well at position 3, located in the center of the room. At near-wall region with relatively high gradient (position 5), both 3D FFD and laminar CFD could not obtain a good agreement with the experiment data. Similarly, Wang and Chen (2009) also found that the CFD simulation with turbulence models did not do a good job at position 5. This was because the flow structure was much complex near the right wall, where separation occurred.

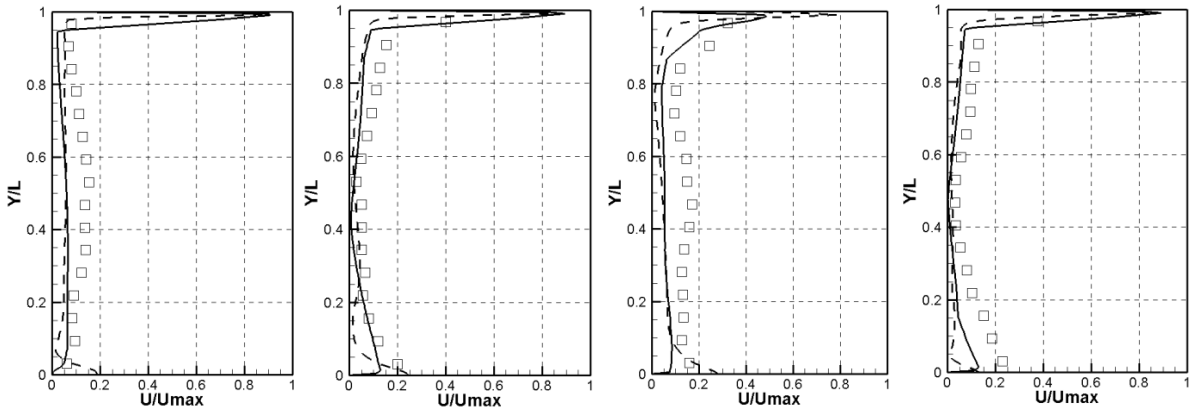


*Figure 4 Comparison of velocity profiles in case A predicted by 3D FFD and CFD with the experiment data at positions (a) 1, (b) 3, (c) 5, and (d) 6, respectively. (Square: Experiment by Wang et al. 2009; Solid line: 3D FFD; Dash line: CFD laminar)*

**Forced convection in the room with box**

In Figure 5, a box with the size of 1.22 m × 1.22 m × 1.22 m was added in the center of the room, and it would cause airflow separation that was similar as the airflow in a room blocked by obstacles like furniture and occupants. So in this case, 3D FFD could be further tested with increasing airflow features and more complex geometry of computational domain. Similarly, this test case was also simulated with laminar CFD using ANSYS FLUENT 12.1, and the grid size of 20×20×20 was used for both 3D FFD and laminar CFD simulations.

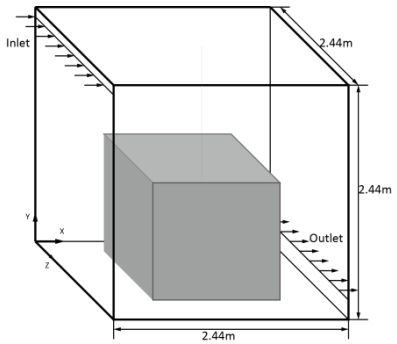


*Figure 1 Schematic of the test room with a box*

Figure 6 reported the velocity profiles at the four locations predicted by 3D FFD and laminar CFD simulations. Compared with the experiment data, 3D FFD under predicted the air

velocity at position 1 and 5. This is because the airflow was complex at position 5, where the airflow was blocked by the box and formed a secondary circulation between the box and right wall. At other two positions the agreement was acceptable with only some discrepancies at near-floor-region. Compared with the results of laminar CFD simulation, 3D FFD was even better for this case.

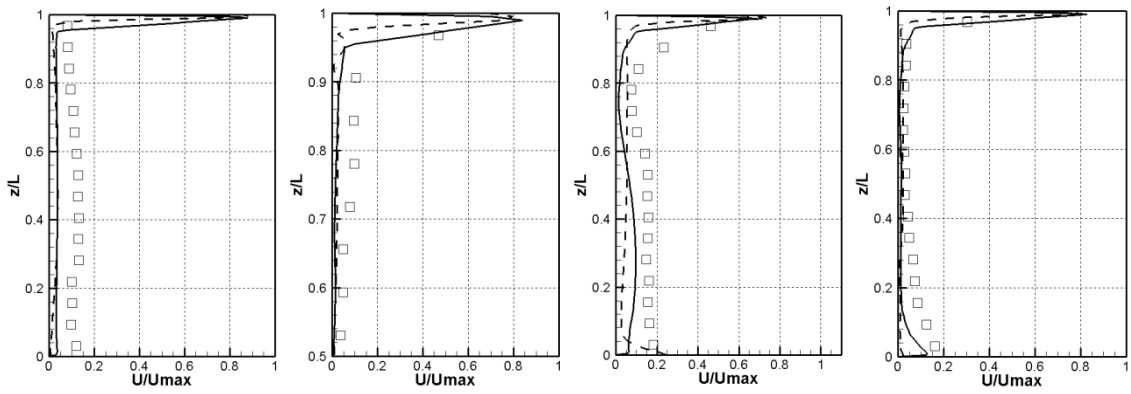


(a) (b) (c) (d)

*Figure 2 Comparison of velocity profiles in case B predicted by 3D FFD and CFD with the experiment data at positions (a) 1, (b) 3, (c) 5, and (d) 6, respectively. (Square: Experiment by Wang et al. 2009; Solid line: 3D FFD; Dash line: CFD laminar)*

**Mixed convection in the room with box**

In Case C, a heat source of 700W was added in the box in Case B. The heated box would generate thermal plumes as often found from different heating sources in buildings, such as occupants and electric appliances, etc. The supply air temperature was controlled at 22.2 $^{o}$C; the temperature of box surface, ceiling, surrounding walls and floor were 36.7, 25.8, 27.4 and 26.9 $^{o}$C, respectively. All other boundary conditions were the same as Case B. The grid size of 20 × 20 × 20 was used for both 3D FFD and laminar CFD simulation in this case.

In Figure 7, the vertical velocity profiles predicted by 3D FFD showed very good agreement with the experimental data except at position 5. Similar to Case B, the failure of 3D FFD at position 5 might caused by its incapability of modeling complex flow structure. Compared with the results of CFD simulations, 3D FFD obtained more accurate results than laminar CFD.

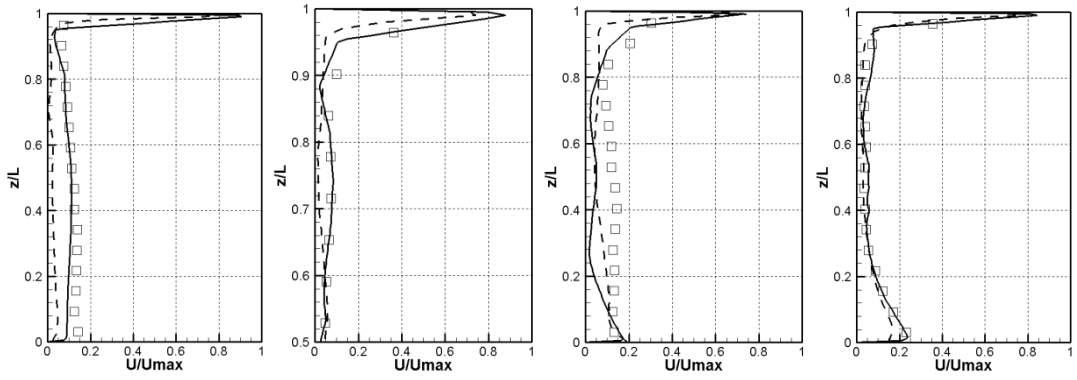


(a) (b) (c) (d)

*Figure 7 Comparison of velocity profiles in case C predicted by 3D FFD and CFD with the experiment data at positions (a) 1, (b) 3, (c) 5, and (d) 6, respectively. (Square: Experiment by Wang et al. 2009; Solid line: 3D FFD; Dash line: CFD laminar)*

This case was non-isothermal so the temperature profiles predicted was compared with the experimental data in Figure 8 at the four positions. At these positions, although the result of 3D FFD was not in perfect agreement with the experimental data, it was still acceptable that it predicted correct temperature magnitude and captured the general vertical variation of temperature. Because of lack of turbulence model, the laminar CFD could not predict the surface heat transfer coefficient correctly and thus under predicted the temperature magnitude. While in 3D FFD, an ad-hoc treatment was applied to adjust the surface heat transfer coefficient so 3D FFD could achieved a better prediction for temperature than laminar CFD.

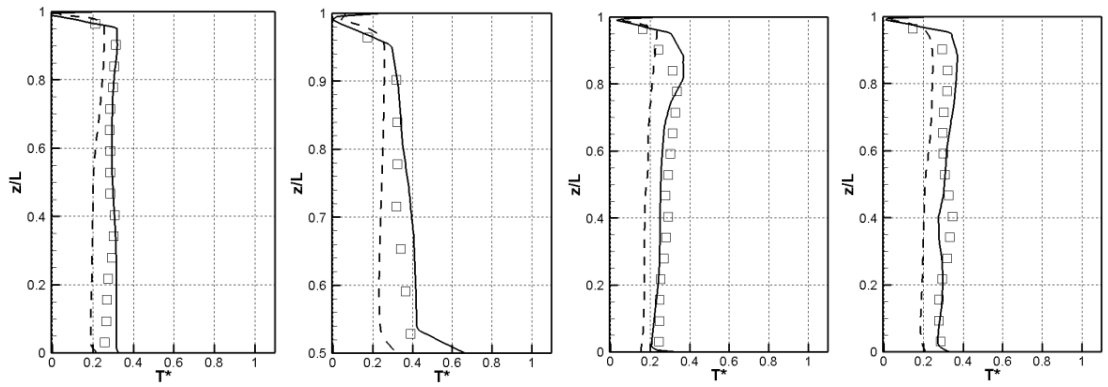


(a) (b) (c) (d)

*Figure 8 Comparison of temperature profiles in case C predicted by 3D FFD and CFD with the experiment data at positions (a) 1, (b) 3, (c) 5, and (d) 6, respectively. (Square: Experiment by Wang et al. 2009; Solid line: 3D FFD; Dash line: CFD laminar)*

## DISCUSSION

The major advantage of the FFD compared to CFD is its speed. This study conducted a comparison of simulation speed between 3D FFD and laminar CFD. Table 1 reported the computing time of the test cases. All three cases used same time step size of 0.1 seconds and grid size of 20 × 20 × 20, and both 3D FFD and laminar CFD simulations were performed on a personal computer with a single Intel CPU at 3.00 GHz. Comparing the elapsed flow time and the elapsed CPU time, 3D FFD could realize faster-than-real time simulations for the grid size and time steps. On the other hand, laminar CFD was 14-18 times slower than 3D FFD.

*Table 1 Comparison of computing time by 3D FFD and laminar CFD*

| Test cases | Elapsed flow time (s) | Elapsed CPU time (s) | |
|---|---|---|---|
| | | 3D FFD | CFD |
| Forced convection in empty room | 100 | 29 | 474 |
| Forced convection in room with box | 100 | 31 | 439 |
| Mixed convection in room with box | 100 | 31 | 555 |

## CONCLUSIONS

In this study, the three dimensional fast fluid dynamics was developed from a two dimensional model. The implementation of boundary conditions and near wall treatment for Semi-Lagrangian method was improved. Through the validation of 3D FFD with three cases of indoor airflows, this study found that 3D FFD could provide reliable and acceptably

accurate simulations for airflows in buildings. The computing speed of the 3D FFD was about 15 times faster than CFD.

## REFERENCES

ANSYS, ANSYS FLUENT 12.1 Documentation, ANSYS Inc., PA.

Chen Q. 2009. Ventilation performance prediction for buildings: A method overview and recent applications. *Building and Environment*, vol. 44, pp. 848-858.

Kim Y. B. and Lee M. J. 2002. Boundary-condition pairs for fractional step methods and compatibility with the pressure Poisson equation. *Computational Fluid Dynamics Journal*, vol. 11, pp. 323-334.

Li P. W. and Tao W. Q. 1994. Effects of outflow boundary condition on convective heat transfer with strong recirculating flow. *HEAT AND MASS TRANSFER*, vol. 29, pp. 463-470, 1994.

Stam J. 1999. Stable fluids. *The 26th annual conference on Computer graphics and interactive techniques*, Los Angeles, 1999, pp. 121-128.

Temam R. 1991. Remark on the pressure boundary condition for the projection method. *Theoretical and Computational Fluid Dynamics*, vol. 3, pp. 181-184.

Wang L. and Chen Q. 2008. Evaluation of some assumptions used in multizone airflow network models. *Building and Environment*, vol. 43, pp. 1671-1677.

Wang M. and Chen Q. 2009. Assessment of various turbulence models for transitional flows in an enclosed environment. *HVAC&R Research*, vol. 15, pp. 1099-1119.

Wood N., Staniforth A. and White A. 2009. Determining near‐boundary departure points in Semi‐Lagrangian models. *Quarterly Journal of the Royal Meteorological Society*, vol. 135, pp. 1890-1896.

Zhai Z. and Chen Q. 2006. Sensitivity analysis and application guides for integrated building energy and CFD simulation. *Energy and Buildings*, vol. 38, pp. 1060-1068.

Zhai Z., Zhang W., Zhang Z. and Chen Q. 2007. Evaluation of Various Turbulence Models in Predicting Airflow and Turbulence in Enclosed Environments by CFD: Part 1--Summary of Prevalent Turbulence Models. *HVAC&R Research*, vol. 13, pp. 853-870.

Zuo W. and Chen Q. 2009. Real‐time or faster‐than‐real‐time simulation of airflow in buildings. *Indoor Air*, vol. 19, pp. 33-44.